Magnetic-assisted self-assembly of rectangular-shaped parts

Dung-An Wang and Hong-Hua Ko

Institute of Precision Engineering, National Chung Hsing University, 250 Kuo Kuang Rd, Taichung 402, Taiwan, Repubic of China

E-mail: daw@dragon.nchu.edu.tw

October 29, 2008

Abstract

A method for self-assembly of millimeter-sized, magnetized, rectangular-shaped parts floating on a molten solder-air interface under a rotating external magnetic field is developed. Rotating magnetic field produces a torque to rotate the magnetized parts into their specific in-plane orientations. The surface tension of the molten solder keeps the parts in these orientations. Experiments are carried out on glass substrates with patterned copper foil. Rectangular binding sites are the only hydrophilic areas on the substrate. By a simple coating process, molten solders wet only the binding sites on the substrate. The parts with orientation angles up to 90° can be rotated and translated to align with the binding sites by the magnetic torque and surface tension. Before the assembly, the solder is reflowed by heating to 80°C. The alignment completed within 27 seconds with a orientation angle of 90°. The integrity of the bonding is confirmed by a static debonding test.

1. Introduction

It is a major challenge to develop assembly methods for meso and micro scale components in complex heterogeneous integrated systems. Assembly of parts has been done by the conventional pick and place robotic assembly [1], microstructure transfer between aligned wafers [2,3], and dynamic self-assembly [4]. Robotic assembly is a serial process and can be subject to adhesion forces resulting from handling and positioning micro/nano components. Wafer-level transfer is an inherently two-dimensional fabrication method and cannot generate truly three-dimensional structures [5]. Self-assembly is generally a batch process where micro-fabricated components are integrated and constructed automatically as functional units. Self-assembly of sophisticated, three-dimensional networks has been demonstrated by Gracias et al. [6] where millimeter-scale polyhedra, with surfaces patterned with solder dots, wires, and light-emitting diodes, were assembled in hot, isodense, aqueous KBr solution.

Parts assembled by self-assembly need a method for the mechanical connection to hold the final structure together and electrical connection between components to make the final assembled structure functional. Different ways can be applied to make the electrical connection between parts. Solders applied by electroplating, screen printing or sputtering can produce reliable electrical connection for wafer to wafer bonding [7]. However, the electrical contacts produced by electroplated solders suffer from poor mechanical properties [8]. Polymer interconnections show great promise as conducting materials in a wide range of application areas due to their tolerance of mechanical stress, ease of processing and their chemical tunability [9]. Nevertheless, their electrical resistivity is high, their contact area may be limited to asperities, and at the molecular level they may be to able to withstand high-temperature processing and operation [5,10]. Soldering processes for assembly of parts to each other or to a substrate has excellent electrical, thermal, and mechanical properties.

Methods of assembling parts using molten solder have been developed with different driving mechanisms [11-17]. Based on surface energy minimization of molten solder balls, Harsh et al. [12] demonstrated an assembly of a hinged plate through control of solder volume. A magnetic field is employed by Ye et al. [17] to integrate nanowires with a solder-padded substrate. Morris and Parviz [15] assembled circular and square micropart to the binding sites on a silicon template in a fluid environment. Orbital shaking assisted self assembly of square PZT parts in an air environment was demonstrated by Fang et al. [11].

In this paper, a simple process to achieve on-substrate self-assembly of millimeter-sized, magnetized, rectangular parts using molten solder is reported. The assembly technique is assisted by a rotating magnet and provides accurate placement of parts in an air environment. A quasi-static model to study complex behavior of a part rotating at a solder-air interface is developed. Experiments are carried out to demonstrate the feasibility of the assembly method. Bonding strength of the assembled part is investigated by a debonding test.

2. Magnetic-assisted self-assembly

Surface tension has been the driving force for the self-assembly technique using molten solder, especially in fluid environment [18,19]. Self-alignment of microparts to binding sites via a layer of molten solder occurs due to surface energy minimization of the solder. In practice, most microparts are rectangular. The number of minimum energy states depends on the width-to-length ratio of the rectangular parts. For solder self-assembly, the total interfacial energy is related to the overlap area between a part and a binding site. Based on calculations of the overlap area carried out by Fang et al. [11], a square part has four preferred in-plane orientations with rotation angle intervals of 90°, where the surface energy has its local minimums. For micro/nano scale parts, the self-assembly process can be driven by surface tension with fluid agitation [15,18] or simply through minimization of the interfacial free energy [18]. With proper agitation in fluid environment, millimeter-sized parts can settle into the orientations with the local minimum surface energy [8,14]. When assembling millimeter-sized parts in air environment, a means to provide external agitation to assist the assembly process is needed.

To assist self-assembly, a rotating magnetic field can be employed to provide a torque to a millimeter-sized, magnetized part. Fig. 1 illustrates the operation steps of the self-assembly process. Fig. 1(a) shows a misaligned part resting on a binding site of a substrate. A nickel layer can be electroplated at the bottom surface of the part to render it ferromagnetic. A permanent magnet is placed at a distance D below the substrate. Another permanent magnet is placed at a distance Δ above the substrate to cause the part to rise into the air in defiance of gravity. When the magnet below the substrate is rotated with an angular velocity Ω, a magnetic torque is applied to the part to align the part with the binding site as shown in Fig. 1(b). For the materials considered in this investigation, the nickel coated part and the solder material applied on the binding site, the surface energy decreases as the overlap area increases in the air environment.

2.1 Quasi-static Model

In order to estimate the torque needed to align the part with the binding site, a simple model giving the torques acting in the system is developed. For a part resided on molten solder, but not yet aligned with a binding site (see Fig. 1(a)), the torque T generated by the magnet and the restoring torque τ introduced by the molten solder due to the surface energy minimization are also shown in the figure. The magnetic torque T and the restoring torque τ can rotate and retard the motion of the part, respectively. Successful alignment of the part to the binding site requires: 1) the maximum magnitude of T is greater than the maximum magnitude of τ at the various orientations of the part before perfect alignment; 2) the maximum magnitude of T is less than the magnitude of τ at the aligned orientation. Requirement 1 allows the magnetic torque to rotate the misaligned part toward its perfect alignment orientation, and requirement 2 assures the fact that the restoring torque keeps the aligned part to stay in its perfect alignment orientation while the magnetic torque still applies a torque to drive the part out of the perfect alignment orientation.

2.1.1 Estimation of the restoring torque

For systems with simple geometry, 2D analytical models have been used to determine the surface force [20]. For systems with complex shapes, numerical simulations can model the 3D surface and nonlinear effects better than 2D analytical models. A freely available software, Surface Evolver [21,22], can be used to obtain the minimal energy surface. Here, we used the software for efficient estimation of the potential energy during the assembly process. The restoring torque τ can be computed through a smooth perturbation of the potential energy curve with respect to an orientation angle θ of a part, where θ is the measure of an angle with initial side along the length direction of the binding site and terminal side along the length direction of the part as shown in the inset of Fig. 1(a). The following assumptions are made in estimation of the restoring torque applied to a part.

- A part residing on molten solder is not tilted.
- A part does not touch the substrate.
- The motion of a part in the direction perpendicular to the substrate is minimal.
- The shape of a part and a binding site is identical.
- Molten solder wets the hydrophilic surfaces of a part and a binding site completely and exclusively.

The surface energy between the solder and the solid surfaces are the input parameters to the software, Surface Evolver, in order to obtain the minimal energy surface. The values of surface energies γ between molten solder and solid surfaces of the part and the binding site are given as [23]

$$\gamma_{Si} = \gamma_{iA} - \gamma_{SA} \cos\phi \qquad (1)$$

where γ_{Si} is the interfacial energy between solder and solid surface i. γ_{iA} is the surface energy between solid surface i and air environment, and γ_{SA} is the surface energy between solder and air environment. ϕ is the contact angle between molten solder and the solid surfaces. In this investigation, solder, part, binding site and air environment are denoted by S, P, B and A, respectively. The value of γ_{SA} can be measured by a goniometer.

Surface Evolver can evolve the initial shape toward a minimum energy profile. Given the device constraints (volume and density of the solder, mass of the part, wetted areas, and gravity), the initial shape does not need to closely approximate the final shape as long as the constraints are set appropriately [12]. The stable shape and corresponding minimum potential energy can be calculated for each orientation angle of the part. We can then use the potential curve to calculate the restoring torque τ acting on the part at different orientation angles.

2.1.2 Estimation of the magnetic torque

In order to estimate the magnetic torque applied to the part by the magnets, 3D finite element computations are performed. Consider a rectangular magnet P below the part and a rectangular magnet Q above the part as shown in Fig. 1(a). The magnet P with length L_P, width W_P and height H_P has a magnetization vector M_P along its length direction. The magnet Q with length L_Q, width W_Q and height H_Q has a magnetization vector M_Q along its length direction.

In this investigation, Ansoft's Maxwell 3D finite element field simulator is employed to perform the computations. The magnet P, magnet Q and part have 5907, 2138 and 439 tetrahedral elements, respectively. The part, magnet P and magnet Q are enclosed by a region, which defines the outer boundary of the problem. The magnetic field intensity is tangential to the boundary and the magnetic flux cannot cross it. 38375 tetrahedral elements are used for the region. Magnetic torque calculations are based on the virtual work principle using the local Jacobian derivative [24].

2.2 Analysis

The minimal energy surface during the self-assembly process is numerically calculated to predict the restoring torque applied to the part by molten solder. A rectangular part with width $W = 5$ mm, length $L = 10$ mm and thickness $t = 0.2$ mm is considered. The rectangular shaped binding site has exactly the same lateral dimensions as the part. Molten solder of controlled volume of 0.1 cm^3 wets the binding site. Complete wetting of the binding site is assumed. The value of γ_{SA} used in the numerical investigation is 503 dyne/cm, measured by experiments. The values of surface energy between air and the solid surfaces of nickel and silica are taken as 1850 dyne/cm, γ_{PA}, [25] and 300 dyne/cm, γ_{BA} [26], respectively. The contact angles between solder and the solid surfaces of nickel and silica are taken as 70° and 35°, respectively, based on the experiments carried out in this investigation. Using Eq. (1), the values of γ_{SP} and γ_{SB} are calculated as 2206 and 49 dyne/cm, respectively.

Using the software, Surface Evolver, the total surface energies for different orientations are calculated. The maximums of the surface energy lie at the position of perfect alignment. The restoring torque has its maximum magnitude of 450 $\text{dyne}\cdot\text{cm}$ at the orientations near perfect alignment. The minimum magnitude of the restoring torque is 2.6 $\text{dyne}\cdot\text{cm}$ at $\theta = 90^\circ$.

In order to predict the magnetic torque applied to the part, the magnets P and Q with $L_P \times W_P \times H_P = 18$ x 13 x 6 mm, and $L_Q \times W_Q \times H_Q = 40$ x 10 x 7 mm, respectively, are employed in the simulations. The magnets P and Q are magnetized along their longest dimension and have magnetizations $M_P \approx 970845\,\text{A/m}$ and $M_Q \approx 159155\,\text{A/m}$, respectively. The magnetic coercivity of the magnets P and Q are -927 and -125 kA/m, respectively. The distance D between the magnet P and the substrate is taken as 8 mm. The distance Δ between the magnet Q and the substrate is taken as 10 mm. The relative permeability of the part is taken as 600. Fig. 2 shows the magnetic torques as functions of the angle of the rotated magnet P based on the finite element computations performed here. Three orientation angles of the part, namely, 0°, 45° and 90°, are considered. As shown in the figure, the magnetic torques applied to the part are between -260 and 260 $\text{dyne}\cdot\text{cm}$, for the three orientation angles of the part considered. Due to geometric symmetry, the magnetic torques for all orientations of the part should be in the range of -260 to 260 $\text{dyne}\cdot\text{cm}$.

The results indicate that for the selected magnetic properties and geometry of the part and magnets, the maximum magnitude of the magnetic torque for different rotation angles of the magnet P is well below the magnitude of the restoring torque when the part is in perfect alignment with the binding site. Since the value of the magnetic torque ranges from -260 to 260 $\text{dyne}\cdot\text{cm}$, the misaligned part with different orientation angles can be rotated towards the perfect alignment with the binding site, and stay in that orientation under the quasi-static condition. Note that the inertial and damping effects due to the rotation of the part and the magnets are not considered in the analyses. The analyses presented here serve as a design guideline of the part and magnets used for this self-assembly method.

3. Experiment

3.1 Fabrication of binding sites

The binding site is designed as a rectangular hydrophilic well in a hydrophobic surface. The well is later coated with molten solder. To establish the binding site on a glass substrate, first a 5 × 10 mm rectangular pattern is cut out of a copper foil of thickness 0.4 mm by milling. Then, the patterned foil is attached to a glass substrate to form the hydrophobic surface. The binding site on the glass substrate is the hydrophilic surface.

3.2 Fabrication of parts

5 × 10 × 0.2 mm rectangular electroplated nickel parts are chosen for demonstration of the presented self-assembly method. Nickel is selected due to its relatively high magnetic permeability and mechanical stiffness. The rectangular shape has two preferred in-plane orientations with rotation angle interval of 180°. Compared to square parts which have four preferred in-plane orientations, rectangular parts are good candidates to test the orientation capability of the presented method. Nickel parts are fabricated using a simple electroforming process. First, an electroplating tape is attached to a stainless steel substrate. Then, a rectangular pattern is cut out of the tape. Next, a 200 μm-thick nickel layer is electrodeposited using a low-stress nickel sulfamate bath with the chemical compositions listed in Table 1. The bath is kept at a temperature of 45°C and a pH value around 4.6. A 10-minute nickel strike is carried out with the current density of 1 A/dm^2, followed by a 7-hour nickel plating with the current density

of 2 A/dm^2. Then, the electroplating tape is detached from the substrate. Finally, the electroplated nickel layer is removed from the substrate by a thin slide.

3.3 Solder coating process

Solder is applied on the binding site with a simple coating process. A container for housing the solder is placed onto a hot plate and heated at $100^{\circ}C$ until it is melted. The molten solder is manually dropped into the binding site and wets only the hydrophilic binding site. Figs. 3(a) and (b) show a patterned substrate before and after the coating process, respectively. Fig. 3(a) shows a recessed hydrophilic well in a hydrophobic Cu surface. As shown in Fig. 3(b), after the coating process, only the hydrophilic binding site is coated with the molten solder. The amount of the solder coated on the binding site is estimated as $0.1\ cm^3$.

3.4 Magnetic- assisted self-assembly

The fabricated parts are tested using the experimental apparatus shown in Fig. 4. A speed control unit is integrated into a motor to adjust the angular velocity of the magnet P of NdFeB (ND-36, Magtech Magnetic Products Co., Taiwan). An acrylic fixture is used to hold the magnet Q of ferrite (Y8T, Taiwan Magnetic Co., Taiwan). The dimensions and magnetic properties of the magnets P and Q are presented in Section 2.2. The temperature of the heating plate can be set to the desired level by the temperature control unit. A high speed CCD camera (ST-EP130M-C, EPIX, Inc., US) mounted on top of an objective lens (34-11-10, OPPEM) is used for capturing the successive images of the self-assembly process. Using computerized frame-by-frame analysis of captured images, the time for alignment of the parts is measured. A glass substrate containing the patterned copper foil is attached on a heating plate that keeps the solder in molten state. The heating plate is heated at $80\,^{\circ}\mathrm{C}$ during the self-assembly process. The low-temperature solder used in this investigation has a melting point of $72\,^{\circ}\mathrm{C}$.

4. Results and discussions

Magnetic-assisted self-assembly of electroplated nickel parts are performed using the described self-assembly system. The part is introduced manually without alignment onto the solder. By heating the solder on the heating plate with a temperature of $80\,^{\circ}\mathrm{C}$ and with a magnetic torque provided by a rotating magnet, the part can align with the recessed binding site.

4.1 Effects of orientation angle

In order to demonstrate the capability of the self-assembly technique, experiments for parts with the orientation angles of 15°, 30°, 45°, 60°, 75° and 90° are carried out at room temperature in the air environment. The temperature of the heating plate is set to be $80\,^{\circ}\mathrm{C}$. The angular velocity of the rotating magnet, Ω, ranges from 202 to 292 rpm during the assembly process for different orientation angles of the part. Table 2 lists the average angular velocities of five runs for each orientation angle.

Fig. 5 show sequences of snapshots from experiments for $\theta = 90^{\circ}$. For a part with a large θ up to 90°, the self-assembly is completed within 26.5 sec. During the experiments, it is observed that once alignment between parts and binding sites is achieved, the parts are kept aligned with the binding sites without oscillation. Ten data sets of successful runs are recorded for each orientation angle and plotted in Fig. 6. The error bars in Fig. 6 indicate the variation in the experimental results. As shown in Fig. 6, the time to alignment increases as the orientation angle θ increases. Given the seemingly sine curve of the magnetic torque and the highly nonlinear restoring torque, the dynamic behavior of the part is complicated. The experimental observations suggest that there is a relatively slow movement of the part before the part reaches an orientation, which is close to 50°, during alignment process. After the part passes through this orientation, it moves into the perfect alignment relatively quickly. Based on the computational results by the software, Surface Evolver, the restoring torque has a local maximum near the 50° orientation angle of the part. Once the part passes through this local energy barrier, the part gains enough momentum from the rotating magnet and move into the perfect alignment quickly.

The assembly yield with respect to the orientation angle is plotted in Fig. 7. The yields of the self-assembly for the six orientation angles ranging from 15° to 90° are at least 70%. A negative trend of a nearly flat slope in yield is observed as the orientation angle increases. The effectiveness of the self-assembly technique developed here is confirmed by the high yields observed in the experiments, even for the large orientation angles. It is noted that most failed parts with initial orientation angles less than or equal to 45° stick to their initial orientations regardless the different angular speeds of the rotating magnet. When the part is manually placed onto the solder, it might be slightly tilted. The alignment failure may be attributed to the tilting of the part. For the failed parts with initial orientation angles greater than or equal to 60°, most of them stop at the orientation angles near 50°. Since the restoring torque has a local maximum near the 50° orientation angle of the part, it is thought that the magnetic torque provided by the rotating magnet could not overcome this local energy barrier.

4.2 Effects of shift displacement

Due to the fact that the parts are manually placed onto the molten solder, the geometry center of the part might not coincide with that of the binding site. In order to examine the effects of the shift displacement of parts on the assembly yield, experiments for shifted parts are performed. Fig. 8 shows photos of shifted parts with orientation angle $\theta = 90^\circ$. Fig. 8(a) shows a shifted part and a Cartesian coordinate system. Figs. 8(b), (c) and (d) show parts for the shift displacements of -1.65, 0, and 1.65 mm, respectively. The yields for the self-assembly of parts with five shift displacements are plotted in Fig. 9. The angular velocity of the rotating magnet is set to 280 rpm in the experiments. For parts with the shift displacements of -1.65 and 1.65 mm, the yields are higher than 60%. As the shift displacement increases to -3 and 3 mm, self-assembly of the parts is not successful. The molten solder on the binding site has a curved surface. Near the edge of the binding site, the curved surface has a larger curvature than the curved surface near the center of the binding site. For the parts with a shift displacement of -3 and 3 mm, they are tilted significantly. The unsuccessful alignment is attributed to this initial tilting of the part. The unaligned part may tilt and touch the substrate with their corners or edges which prevents the part from rotating toward its perfect alignment.

Experiments carried out in this investigation reveal that no successful run of the self-assembly of the parts is observed when the angular velocity of the rotating magnet is lower than 280 rpm. Based on experimental observations, for the successful runs, the shifted parts are rotated quickly and swung into perfect alignment. The alignment for these shifted parts may be achieved by the higher angular momentum provided by the rotating magnet with higher angular speeds. The angular speed of the rotating magnet, 280 rpm, appears to be the threshold value for successful alignment of the parts shifted 1.65 mm.

4.3 Wettability of solder

In order to understand the wettability of the solder used in the experiments, contact angles of the molten solder on different surfaces are measured by a FTA200 goniometer (First Ten Angstroms, Inc.) in an air environment. For comparison, contact angles of water on different surfaces are also measured. The pressure and temperature of the droplet ejector are adjusted for contact angle measurements. The droplet ejector is heated to 90°C to melt the solder by a heating coil wrapped around the exterior surface of the ejector. The results, listed in Table 3, indicate that the surface of the electroplated nickel is hydrophilic, and the glass surface has much higher attraction than Cu coated glass for water and the molten solder. As demonstrated in the experiments, the molten solder only wets the glass binding sites on the Cu patterned glass substrate during the solder coating process.

In order to confirm the effective bonding between the part and the binding site, debonding tests are performed. A glass substrate with an aligned part is held vertically by a fixture. The probe tip of a force gauge (FG5020, Lutron Electronic Enterprise Co., Ltd., Taiwan) is pushed against an edge surface of the part. A pressing force applied to the part is increased until the part is debonded, and the final reading of the force gauge is taken as the debonding force. Four parts assembled are respectively debonded by forces of 4.75 N, 4.70 N, 4.45 N and 4.15 N. The experimental results indicate that the strength of the bonding is quite uniform. Fang et al. [11] reported a debonding force of nearly 6 N in average for their self-assembled 3-mm square PZT parts with an adhesive by an in-water assembly process.

5. Conclusions

This paper presented a method for an on-substrate self-assembly of parts in an air environment. Magnetized millimeter-sized parts are assembled to the corresponding binding sites using molten solder and a rotating magnet. Precise alignment of the parts with orientation angle up to 90° is achieved with a yield up to 70%. The alignment process is completed within 27 seconds. The debonding strength is confirmed by a static debonding test. This assembly technique provides precise placement of rectangular parts with a high width-to-length ratio by magnetic-assisted self-assembly. The high-yield self-assembly approach, achieved without precise control of solder volume and complex robotic manipulation, would further shorten production time and lower packaging cost.

Acknowledgement

This work was financially supported by National Science Council, Taiwan (Grant Number: NSC 96-2221-E-005-095). The authors would like to express their appreciation to the National Center for High-Performance Computing (NCHC), Taiwan for their assistance.

References

[1] K. Mølhave, T.M. Hansen, D.N. Madsen, P. Bøggild, Towards pick-and-place assembly of nanostructures, Journal of Nanoscience and Nanotechnology 4 (2004) 279-282.

[2] A.S. Holmes, S.M. Saidam, Sacrificial layer process with laser-driven release for batch assembly operations, Journal of Microelectromechanical Systems 7 (1998) 416-422.

[3] A. Singh, D.A. Horsley, M.B. Cohn, A.P. Pisano, R.T. Howe, Batch transfer of microstructures using flip-chip solder bonding, Journal of Microelectromechanical Systems 8 (1999) 27-33.

[4] B.A. Grzybowski, M. Radkowski, C.J. Campbell, J.N. Lee, G.M. Whitesides, Self-assembling fluidic machines, Applied Physics Letters 84 (2004) 1798-1800.

[5] E. Saeedi, S. Abbasi, K. Böhringer, B.A. Parviz, Molten-alloy driven self-assembly for nano and micro scale system integration, Fluid Dynamics & Materials Processing 2 (2006) 221-245.

[6] D.H. Gracias, J. Tien, T.L. Breen, C. Hsu, G.M. Whitesides, Forming electrical networks in three dimensions by self-assembly, Science 289 (2000) 1170-1172.

[7] D. Sparks, G. Queen, R. Weston, G. Woodward, M. Putty, L. Jordan, S. Zarabadi, K. Jayakar, Wafer-to-wafer bonding of nonplanarized MEMS surfaces using solder, J. Micromech. Microeng 11 (2001) 630-634.

[8] X. Xiong, Y. Hanein, J. Fang, Y. Wang, W. Wang, T. Daniel, D.T. Schwartz, K.F. Böhringer, Controlled multibatch self-assembly of microdevices, Journal of Microelectromechanical Systems 12 (2003) 117-127.

[9] C. Videlot, J. Ackermann, F. Fages, T.N. Nguyen, L. Wang, P.M. Sarro, D. Crawley, K. Nikolić, M. Forshaw, Polymer interconnections for 3D-chip stacking technology: directional volume patterning of flexible substrates with conducting polymer wires, J. Micromech. Microeng. 14 (2004) 1618-1624.

[10] R.L. McCreery, Molecular electronic junctions, Chem. Mater. 16 (2004) 4477-4496.

[11] J. Fang, K. Wang, K.F. Böhringer, Self-assembly of PZT actuators for micropumps with high process repeatability, Journal of Microelectromechanical Systems 15 (2006) 871-878.

[12] K.F. Harsh, V.M. Bright, Y.C. Lee, Solder self-assembly for three-dimensional microelectromechanical systems, Sensors and Actuators 77 (1999) 237-244.

[13] H.O. Jacobs, A.R. Tao, A. Schwartz, D.H. Gracias, G.M. Whitesides, Fabrication of a cylindrical display by patterned assembly, Science 296 (2002) 323-325.

[14] M. Liu, W.M. Lau, J. Yang, On-demand multi-batch self-assembly of hybrid MEMS by patterning solders of different melting points, J. Micromech. Microeng. 17 (2007) 2163-2168.

[15] C.J. Morris, B.A. Parviz, Micro-scale metal contacts for capillary force-driven self-assembly, J. Micromech. Microeng. 18 (2008) 015022.

[16] S.A. Stauth, B.A. Parviz, Self-assembled silicon networks on plastic. In: Proc. 13th Int. Conf. on Solid State Sensors Actuators (Transducers ’05), Seoul, Korea, 2005, pp 964-967.

[17] H. Ye, Z. Gu, T. Yu, D.H. Gracias, Integrating nanowires with substrates using directed assembly and nanoscale soldering, IEEE Transactions on Nanotechnology 5 (2006) 62-66.

[18] J. Chung, W. Zheng, T.J. Hatch, H.O. Jacobs, Programmable reconfigurable self-assembly: parallel heterogeneous integration of chip-scale components on planar and non planar surfaces, Journal of Microelectromechanical Systems 15 (2006) 457-464.

[19] K.L. Scott, T. Hirano, H. Yang, H. Singh, R.T. Howe, A.M. Niknejad, High-performance inductors using capillary based fluidic self-assembly, Journal of Microelectromechanical Systems 13 (2004) 300-309.

[20] J. Lienemann, A. Greiner, J.G. Korvink, X. Xiong, Y. Hanein, K.F. Böhringer, Modelling , simulation and experimentation of a promising new packaging technology – parallel fluidic self-assembly of micro devices, Sensor Update 13 (2003) 3-43.

[21] K.A. Brakke, The surface evolver, Experimental Mathematics 1 (1992) 141-165.

[22] K.A. Brakke, Surface evolver manual, Mathematics Department, Susquehanna University, Selinsgrove, August 18, 1999.

[23] T. Young, An essay on the cohesion of fluids, Phil. Trans. R. Soc. Lond. 95 (1805) 65-87.

[24] J.L. Coulomb, A methodology for the determination of global electromechanical quantities from a finite element analysis and its application to the evaluation of magnetic forces, torques and stiffness, IEEE Transactions on Magnetics 19 (1983) 2514-2519.

[25] G.A. Somorjai, Introduction to chemistry and catalysis, John Wiley & Sons, Inc., New York, 1993.

[26] S.H. Ehrman, Effect of particle size on rate of coalescence of silica nanoparticles,

Journal of Colloid and Interface Science 213 (1999) 258-261.

Biographies

Dung-An Wang received the Ph.D. degree in mechanical engineering from the University of Michigan at Ann Arbor, in 2004. He is currently an Assistant Professor in the Institute of Precision Engineering, National Chung Hsing University, Taiwan, ROC. His research interests include micromachined resonators and actuators, piezoelectric actuators, microassembly and compliant mechanisms.

Hong-Hua Ko received the B.S. degree in mechanical and mechatronic engineering from the National Taiwan Ocean University, Taiwan, ROC, in 2007, and is currently working towards the M.S. degree in the Institute of Precision Engineering, National Chung Hsing University, Taiwan, ROC. His research interests are microassembly and vibration energy harvesters.

List of figures

Fig. 1 Two-step operation of the self-assembly of a part. (a) A rectangular magnet rotates at angular velocity of Ω below a substrate. (b) The resulting alignment of the part.

Fig. 2 Restoring torque as a function of the orientation angle.

Fig. 3 (a) Patterned Cu layer on a substrate. (b) Only the binding site is coated with molten solder.

Fig. 4 A photo of the experimental apparatus.

Fig. 5 Snapshots of self-assembly of a part with $\theta = 90^{\circ}$.

Fig. 6 Alignment time with respect to various orientation angles.

Fig. 7 Alignment yield with respect to various orientation angles.

Fig. 8 Photos of parts with different shift displacements.

Fig. 9 Alignment yield with respect to various shift displacements.

Table 1. Chemical compositions of the low-stress nickel electroplating solution

Chemical	Amount (/L)
Nickel sulfamate, $Ni(NH_2SO_3)_2 \cdot 4H_2O$	330 ml
Nickel chloride, $NiCl_2 \cdot 6H_2O$	4 g
Boric acid, H_3BO_3	40 g
Wetting agent	2 ml

Table 2. Angular velocity of the rotating magnet for various orientation angles

Angular velocity [rpm]	Orientation angle [deg]
214	15
264	30
276	45
280	60
282	75
284	90

Table 3. Contact angles of water and molten solder on different surfaces.

Surface	Water [deg]	Molten solder [deg]
Cu	80	120
Glass	16	35
Ni	60	70

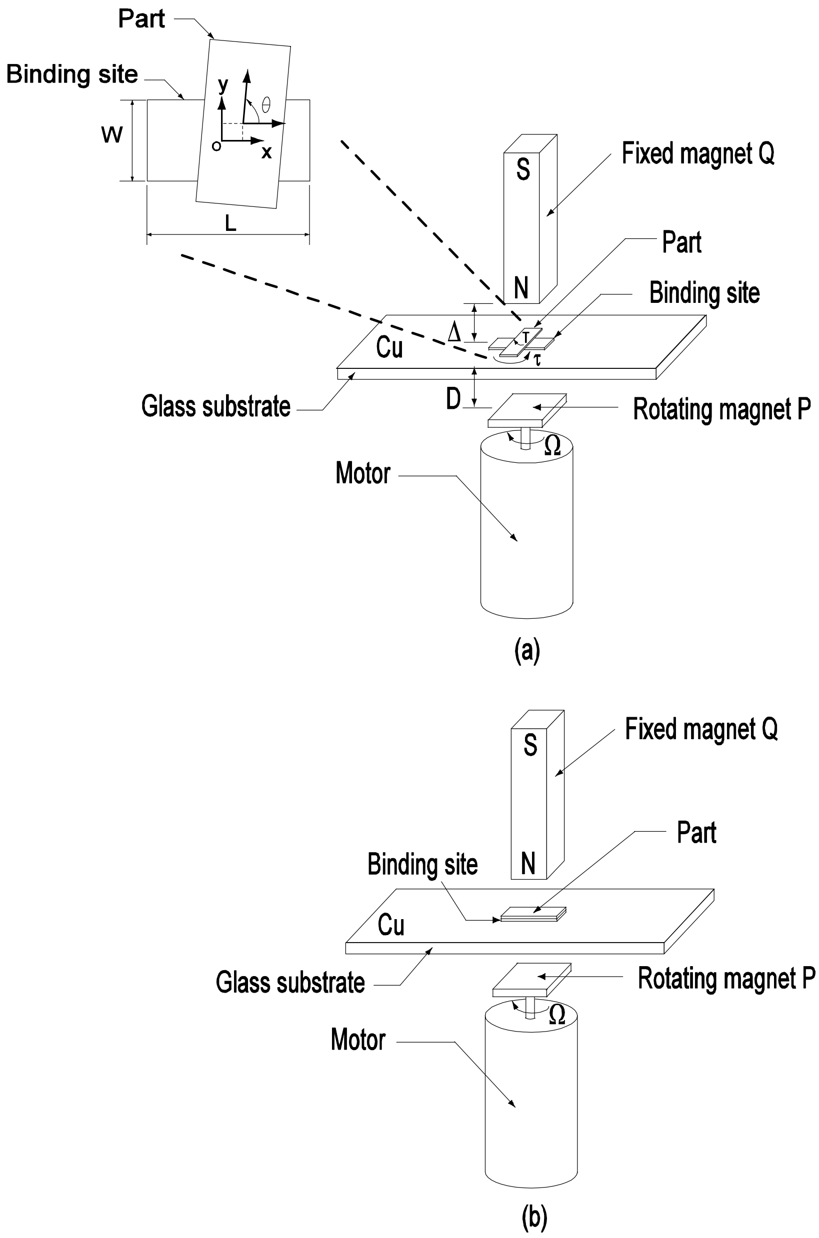

Fig. 1 Two-step operation of the self-assembly of a part. (a) A rectangular magnet rotates at angular velocity of Ω below a substrate. (b) The resulting alignment of the part.

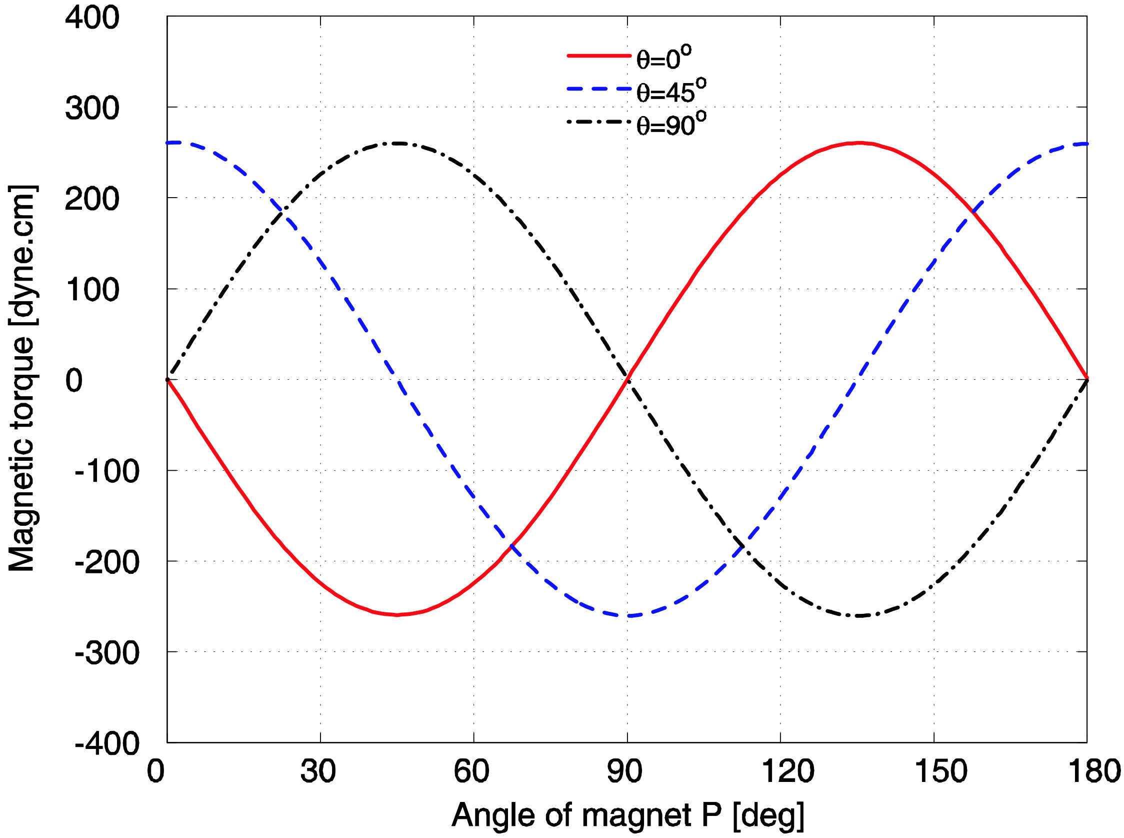

Fig. 2 Restoring torque as a function of the orientation angle.

Fig. 3 (a) Patterned Cu layer on a substrate. (b) Only the binding site is coated with molten solder.

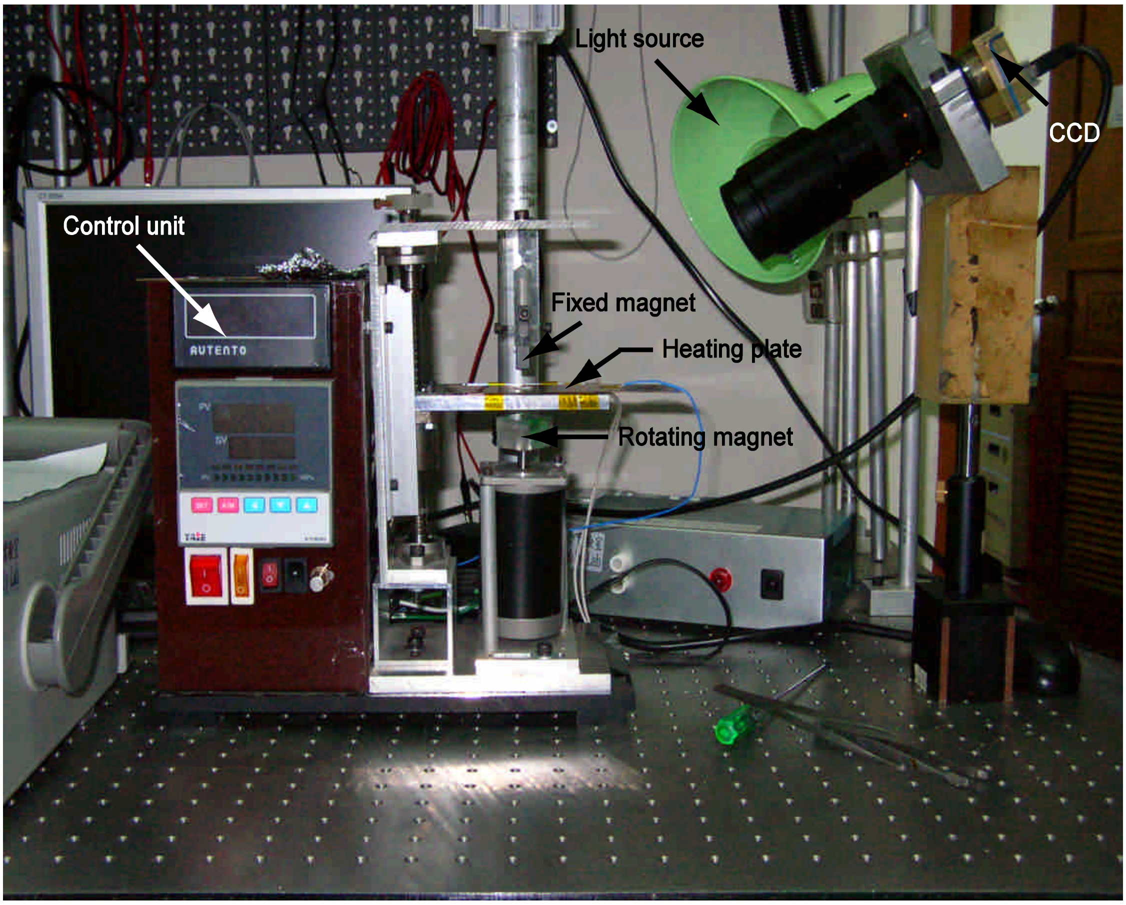

Fig. 4 A photo of the experimental apparatus.

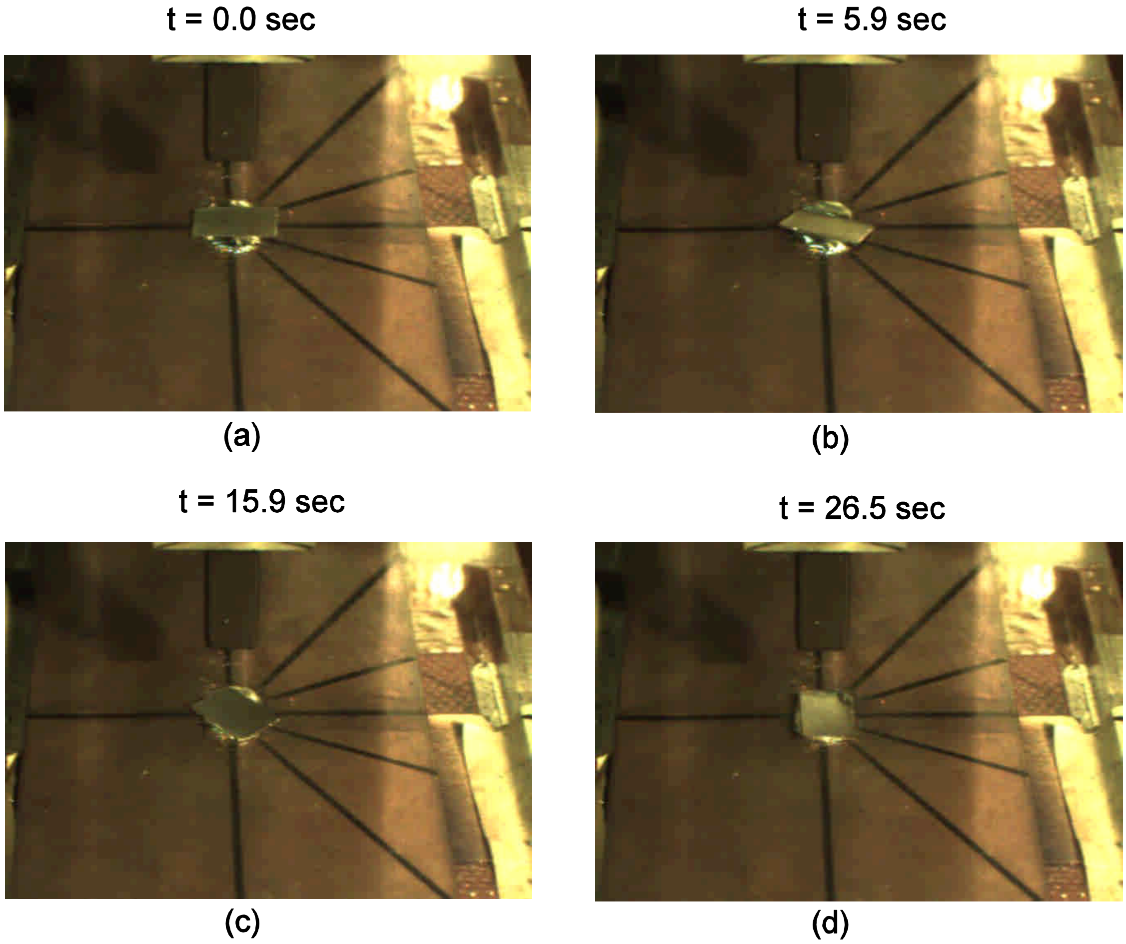

Fig. 5 Snapshots of self-assembly of a part with $\theta = 90^\circ$.

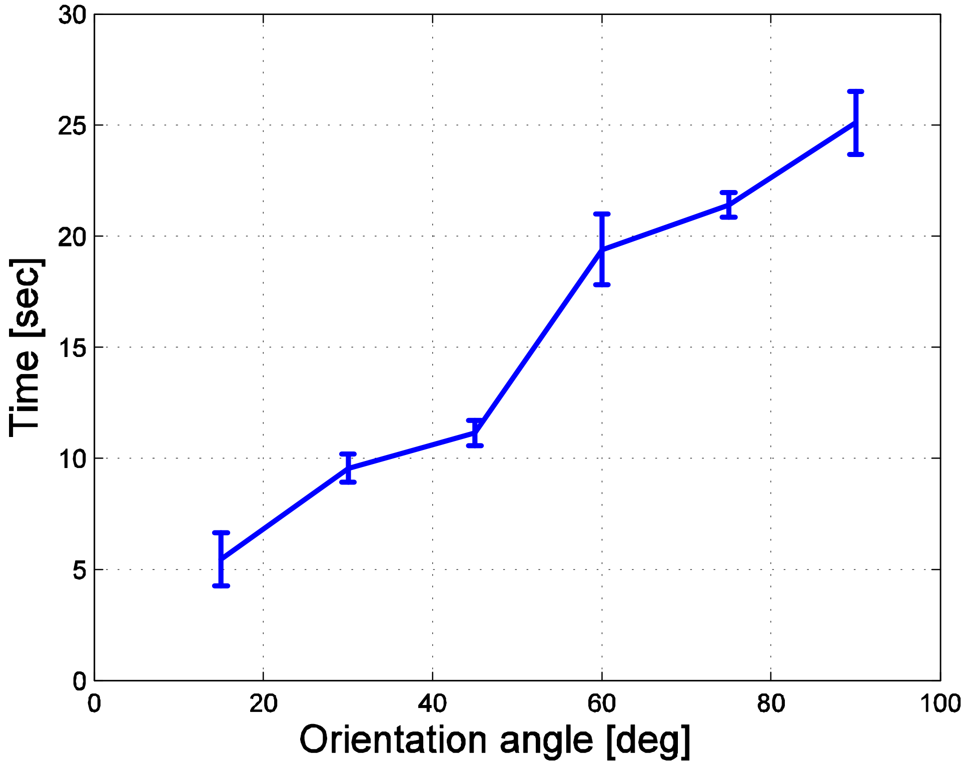

Fig. 6 Alignment time with respect to various orientation angles.

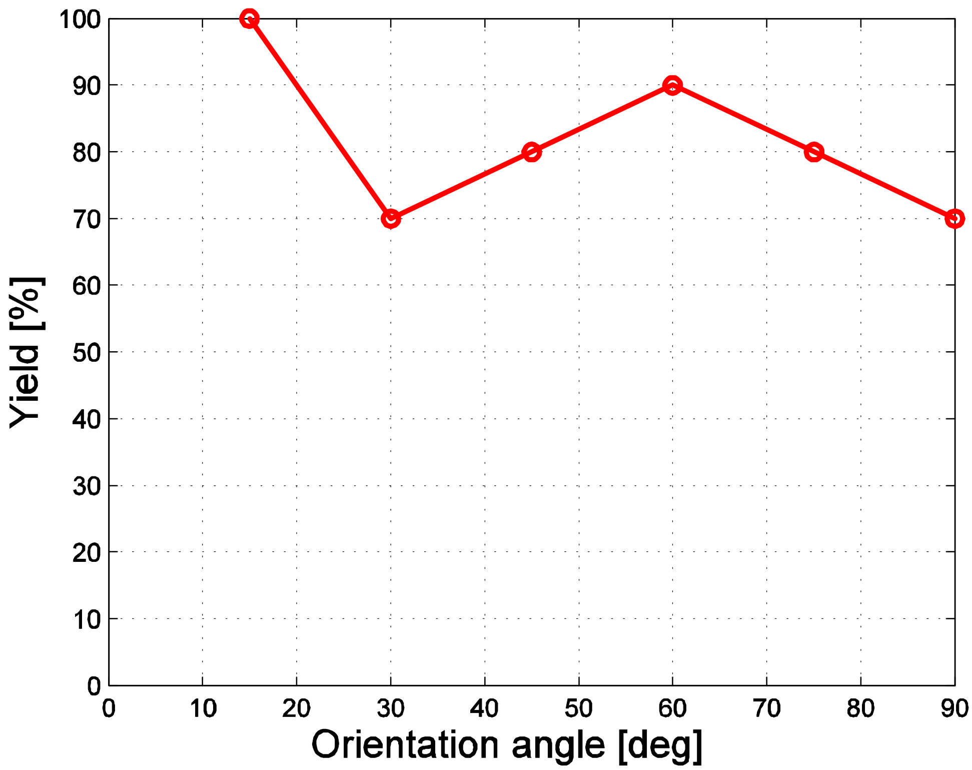

Fig. 7 Alignment yield with respect to various orientation angles.

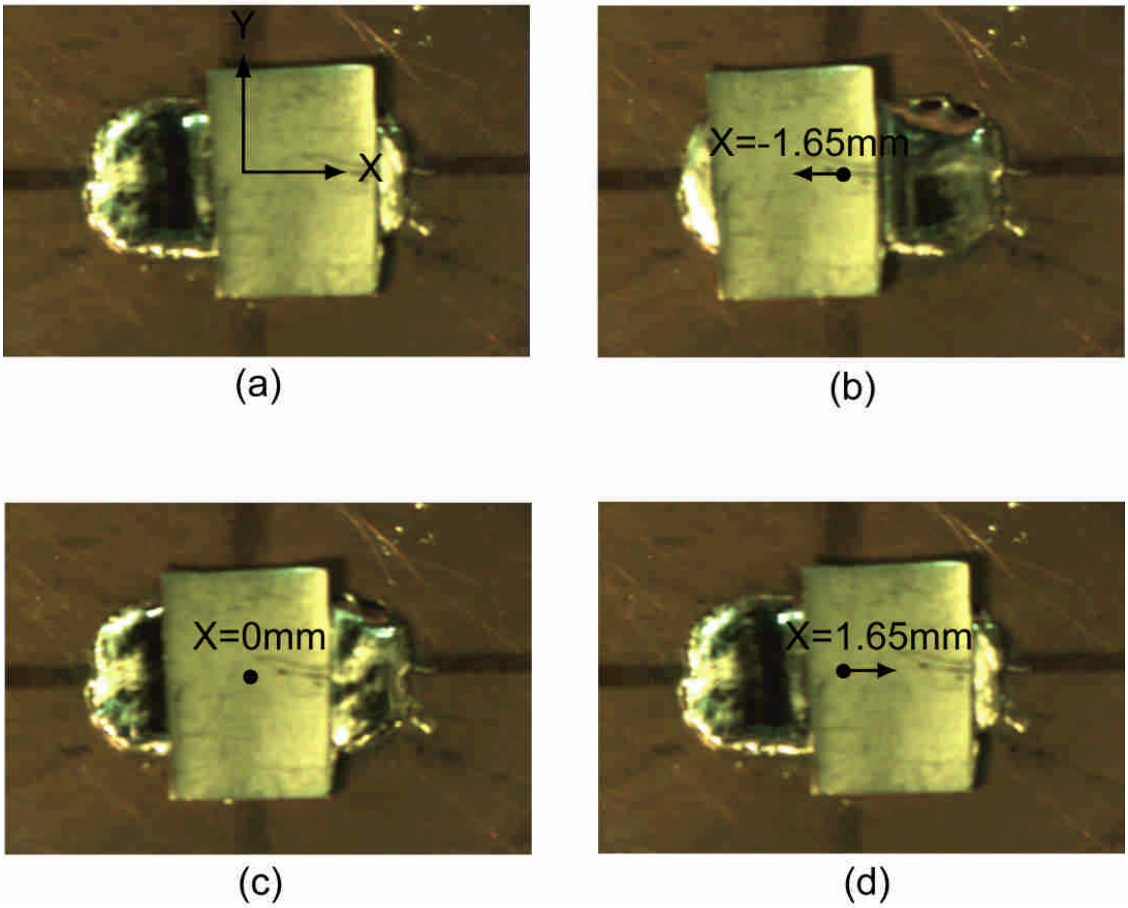

Fig. 8 Photos of parts with different shift displacements.

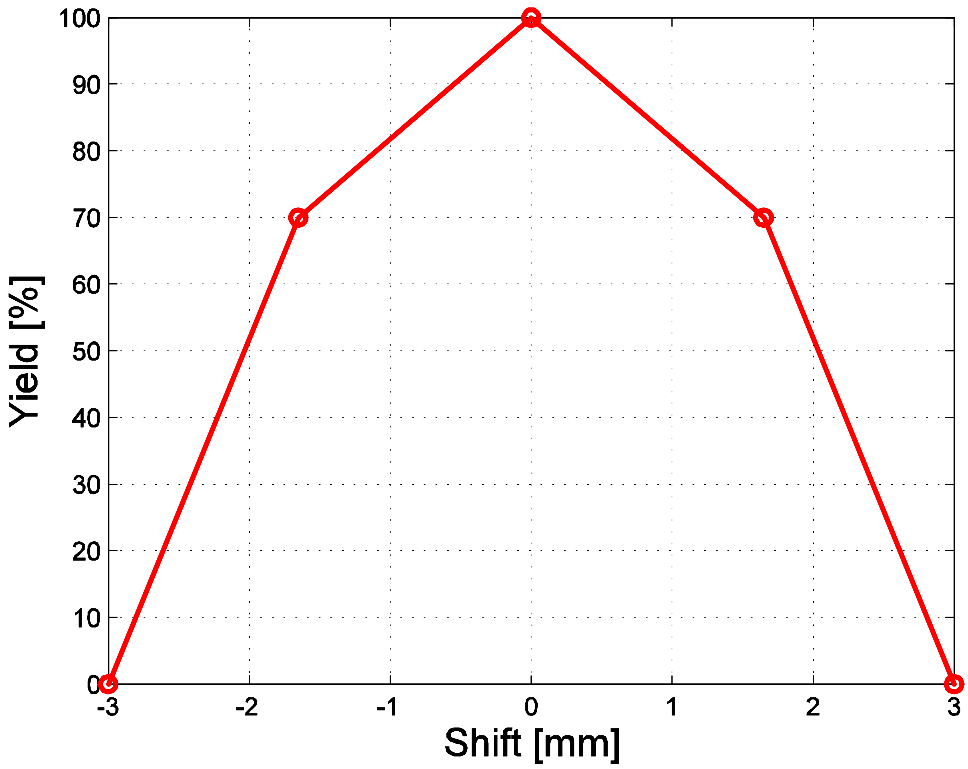

Fig. 9 Alignment yield with respect to various shift displacements.